

# X-RAY EMISSION FROM TWO INFRARED-SELECTED GALAXY CLUSTERS AT $z > 1.4$ IN THE IRAC SHALLOW CLUSTER SURVEY

M. BRODWIN,<sup>1,2</sup> D. STERN,<sup>3</sup> A. VIKHLININ,<sup>1</sup> S. A. STANFORD,<sup>4,5</sup> A. H. GONZALEZ,<sup>6</sup> P. R. EISENHARDT,<sup>3</sup> M. L. N. ASHBY,<sup>1</sup>  
M. BAUTZ,<sup>7</sup> A. DEY,<sup>8</sup> W. R. FORMAN,<sup>1</sup> D. GETTINGS,<sup>6</sup> R. C. HICKOX,<sup>9</sup> B. T. JANNUZI,<sup>8</sup> C. JONES,<sup>1</sup> C. MANCONE,<sup>6</sup>  
E. D. MILLER,<sup>7</sup> L. A. MOUSTAKAS,<sup>3</sup> J. RUEL,<sup>10</sup> G. SNYDER,<sup>1</sup> AND G. ZEIMANN<sup>4</sup>

*Submitted to ApJ*

## ABSTRACT

We report the X-ray detection of two  $z > 1.4$  infrared-selected galaxy clusters from the IRAC Shallow Cluster Survey (ISCS). We present new data from the *Hubble Space Telescope* and the W. M. Keck Observatory that spectroscopically confirm cluster ISCS J1432.4+3250 at  $z = 1.49$ , the most distant of 18 confirmed  $z > 1$  clusters in the ISCS to date. We also present new spectroscopy for ISCS J1438.1+3414, previously reported at  $z = 1.41$ , and measure its dynamical mass. Clusters ISCS J1432.4+3250 and ISCS J1438.1+3414 are detected in 36ks and 143ks *Chandra* exposures at significances of  $5.2\sigma$  and  $9.7\sigma$ , from which we measure total masses of  $\log(M_{200,LX}/M_\odot) = 14.4 \pm 0.2$  and  $14.35^{+0.14}_{-0.11}$ , respectively. The consistency of the X-ray and dynamical properties of these high redshift clusters further demonstrates that the ISCS is robustly detecting massive clusters to at least  $z = 1.5$ .

*Subject headings:* galaxies: clusters: individual (ISCS J1432.4+3250, ISCS J1438.1+3414) — galaxies: distances and redshifts — galaxies: evolution

## 1. INTRODUCTION

Present-day galaxy clusters contain large, old, roughly coeval populations of massive, quiescent galaxies spanning a vast range of local densities. As such, they provide a natural laboratory in which to test models of galaxy formation and evolution. To trace the evolution of cluster galaxies over their full lifetime, it is necessary to identify and study the *precursor* cluster population over a large redshift range. For instance, the Coma cluster, with a present-day mass of  $\log(M_{200}/M_\odot) \approx 15.3$  (Kubo et al. 2007), is expected to have a precursor at  $z \sim 1.5$  with a halo mass of  $\log(M_{200}/M_\odot) \sim 14.6$ . This kind of archaeology requires uniformly selected, well characterized cluster samples in which the evolutionary precursors can be statistically identified, and which are sensitive down to the group scale at very high redshift. Neither X-ray nor Sunyaev-Zel'dovich (SZ) cluster surveys have the mass sensitivity at high redshift, and optical methods fail at  $z \gtrsim 1$  as the red sequence shifts to the infrared.

The *Spitzer*/IRAC Shallow Cluster Survey (ISCS, Eisenhardt et al. 2008) is a stellar mass-selected galaxy

cluster survey spanning  $0.1 < z < 2$ . Clusters are identified via stellar mass overdensities in a  $4.5 \mu\text{m}$ -selected galaxy sample using accurate photometric redshifts (Brodwin et al. 2006), and their selection is therefore independent of the presence of a red sequence. There are 335 clusters and groups in the sample, identified over  $7.25 \text{ deg}^2$  within the Boötes field of the NOAO Deep Wide-Field Survey (Jannuzi and Dey 1999), and 1/3 of the clusters are at  $z > 1$ . The ISCS cluster sample has a mean halo mass, derived from its clustering, of  $\approx 10^{14} M_\odot$  out to  $z = 1.5$  (Brodwin et al. 2007). Cluster photometric redshift accuracy, based on comparison with over 100 clusters spanning  $0 < z < 1.5$ , is excellent, with  $\sigma = 0.028(1+z)$ . At  $z < 1$  roughly 100 clusters have been spectroscopically confirmed, primarily using the extensive spectroscopic database of the AGN and Galaxy Evolution Survey (AGES, Kochanek et al. in prep). To date, we also have spectroscopically confirmed 18 clusters spanning  $1 < z < 1.5$ . (Stanford et al. 2005; Brodwin et al. 2006; Elston et al. 2006; Eisenhardt et al. 2008, Brodwin et al. in prep; Stanford et al. in prep). *All* of the candidates for which adequate spectroscopy has been obtained have turned out to be at the predicted photometric redshifts. The ISCS is therefore the largest sample of spectroscopically confirmed galaxy clusters at  $z > 1$ .

In this paper, we report the X-ray detection of two of the most distant ISCS clusters: ISCS J1438.1+3414 at  $z = 1.414$ , first reported in Stanford et al. (2005), and ISCS J1432.4+3250 at  $z = 1.487$ , for which we present spectroscopic confirmation in this work. The latter is the most distant cluster to date to be spectroscopically confirmed in the ISCS. We present the spectroscopic observations and dynamical properties of these clusters in §2. In §3 we present the X-ray observations, from which we estimate total cluster masses. In §4 we compare the dynamical and X-ray properties of these clusters, including testing the well-known relation between velocity dis-

<sup>1</sup> Harvard-Smithsonian Center for Astrophysics, 60 Garden Street, Cambridge, MA 02138

<sup>2</sup> W. M. Keck Postdoctoral Fellow at the Harvard-Smithsonian Center for Astrophysics

<sup>3</sup> Jet Propulsion Laboratory, California Institute of Technology, Pasadena, CA 91109

<sup>4</sup> Department of Physics, University of California, One Shields Avenue, Davis, CA 95616

<sup>5</sup> Institute of Geophysics and Planetary Physics, Lawrence Livermore National Laboratory, Livermore, CA 94550

<sup>6</sup> Department of Astronomy, University of Florida, Gainesville, FL 32611

<sup>7</sup> Kavli Institute for Astrophysics and Space Research, MIT, Cambridge, MA 02139

<sup>8</sup> NOAO, 950 North Cherry Avenue, Tucson, AZ 85719

<sup>9</sup> Department of Physics, Durham University, South Road, Durham, DH1 3LE, UK

<sup>10</sup> Department of Physics, Harvard University, 17 Oxford Street, Cambridge, MA 02138

persion and temperature at the highest redshift yet. We also discuss the effect of possible systematic uncertainties on our measurements. We present our conclusions in §5. We use Vega magnitudes and a WMAP7+BAO+ $H_0$   $\Lambda$ CDM cosmology (Komatsu et al. 2010):  $\Omega_M = 0.272$ ,  $\Omega_\Lambda = 0.728$ , and  $H_0 = 70.2 \text{ km s}^{-1} \text{ Mpc}^{-1}$ .

## 2. SPECTROSCOPY AND DYNAMICAL MASSES

### 2.1. *ISCS J1438.1+3414*

At the time of its discovery, cluster ISCS J1438.1+3414 at  $z = 1.414$  (Fig. 1), was the most distant galaxy cluster known (Stanford et al. 2005). To place this cluster in a proper evolutionary context, it is imperative to directly measure its total mass. Eisenhardt et al. (2008) previously reported the large stellar mass content in ISCS J1438.1+3414, inferred from the infrared luminosity of its members. Recently, Barbary et al. (2010) published the SN Ia rate from a sample of 25 high redshift clusters selected by X-ray, optical and infrared methods. As the SN Ia rate is proportional to the cluster stellar mass content, these clusters were selected to be the most massive known at high redshift. ISCS J1438.1+3414 is the only cluster in that work found to contain *two* confirmed SNe Ia. These SNe Ia, both hosted by early-type galaxies, are the highest redshift cluster SNe known. These results strongly suggest that ISCS J1438.1+3414 is not a group but rather a bona fide massive cluster, with  $M_{200} > 10^{14} M_\odot$ .

Using a combination of optical multi-object Keck spectroscopy and infrared *HST*/WFC3 grism spectroscopy, we have secured 17 confirmed cluster members in ISCS J1438.1+3414 within a radius of 2 Mpc, listed in Table 1. Spectra with the Low-Resolution Imaging Spectrograph (LRIS; Oke et al. 1995) on Keck I were acquired on UT 2005 June 4 using  $1.3'' \times 10''$  slitlets, the G400/8500 grating on the red side, the D560 dichroic, and the 400/3400 grism on the blue side. The seeing was  $0''.9$  and conditions were clear. The Deep Imaging Multi-Object Spectrograph (DEIMOS; Faber et al. 2003) spectra, acquired on UT 5 April 2007, used the 600ZD grating, the OG550 order sorting filter and  $1''$  slitlets. A complete description of the DEIMOS observations is given in Dawson et al. (2009). The infrared *HST* spectroscopy was obtained on UT 2010 May 22 with the Wide Field Camera 3 (WFC3) using the G141 grism and reduced using the aXe software package (Kümmel et al. 2009). Further details on the spectroscopic observations for both of these clusters will be presented in forthcoming papers.

The redshift histogram of cluster members is shown in Figure 2. From these we calculate a biweight (Beers et al. 1990) velocity dispersion of  $\sigma = 757^{+247}_{-208} \text{ km s}^{-1}$ , including the relativistic correction and the usual correction for velocity errors (Danese et al. 1980). The uncertainty estimates, obtained from bootstrap resampling, represent the 68% confidence interval. Both the gapper (Beers et al. 1990) and simple standard deviation estimates yield essentially identical dispersions. Under the assumption that ISCS J1438.1+3414 is approximately virialized, we use the mass-dispersion relation from Evrard et al. (2008) to infer a dynamical mass of  $\log(M_{200, \text{dyn}}/M_\odot) = 14.4^{+0.3}_{-0.7}$ . This is in excellent agreement with the weak lensing mass,  $\log(M_{200, \text{WL}}/M_\odot) =$

$14.5 \pm 0.3$  (Jee, priv. comm).

### 2.2. *ISCS J1432.4+3250*

Cluster ISCS J1432.4+3250 at  $z = 1.487$  is shown in Figure 3 and Table 1 lists the 8 spectroscopic members secured to date. The LRIS spectra were acquired on UT 2010 May 11 using the G400/8500 grating on the red side, the D680 dichroic, and the 400/3400 grism on the blue side. The seeing was  $0''.8$  and conditions were clear. The WFC3 spectra were obtained on UT 2010 Feb 9 with the G141 grism. Although the redshift histogram, shown in Figure 2, is currently too sparse to allow a meaningful constraint on the velocity dispersion, it illustrates that ISCS J1432.4+3250 has dynamical properties similar to ISCS J1438.1+3414.

## 3. X-RAY OBSERVATIONS

A 145.0 ks observation of ISCS J1438.1+3414 was obtained in October 2009 by S. Andreon using the Advanced CCD Imaging Spectrometer (ACIS-S) on board the *Chandra X-Ray Observatory* (Andreon 2008). Those data were split between an observation of 101.3 ks on UT 2009 October 04 (OBS-ID 10461) and an observation of 43.7 ks on UT 2009 October 09 (OBS-ID 12003). We obtained a 35.0 ks ACIS-I observation of ISCS J1432.4+3250 on UT 2008 October 30 (OBS-ID 10457; PI Stanford). For the current analysis we do not include the shallow 5 ks observations of these fields obtained by the XBoötes survey (Murray et al. 2005) for which our faint targets are off-axis.

We processed the data following standard procedures using the *Chandra* Interactive Analysis of Observations (CIAO; V4.2) software. We initially identified the good time intervals for the exposures, yielding effective exposure times of 144.2 ks for ISCS J1438.1+3414 and 31.1 ks for ISCS J1432.4+3250. Both high redshift clusters are clearly associated with extended X-ray emission in the reduced images. After first masking point sources, we extracted source counts in the 0.6 – 6 keV range within  $1'$  radius apertures of each cluster. This extraction aperture approximately corresponds to 500 kpc at the cluster redshifts. Response matrices and effective areas were then determined for each detected source. We used XSPEC (V12.6.0) to fit the background-subtracted X-ray spectra with the MEKAL hot, diffuse gas model (Mewe et al. 1985) using the Wisconsin photo-electric absorption cross-section (Morrison and McCammon 1983). Metal abundances of 0.3 solar were assumed for both clusters.

Extended X-ray emission was also detected from two additional structures in the deep *Chandra* exposure. These have been identified within the ISCS cluster sample as groups at  $z = 0.65$  and  $z = 0.54$ , and will be further discussed by Miller et al. (in prep).

### 3.1. *ISCS J1438.1+3414*

We measure 312 background-subtracted source counts for cluster ISCS J1438.1+3414, corresponding to a detection significance of  $9.7\sigma$ . The X-ray peak is centered at  $\alpha = 14^{\text{h}}38^{\text{m}}08.3^{\text{s}}$ ,  $\delta = 34^\circ14'15''$  (J2000). Adopting a Galactic  $N_H = 9.94 \times 10^{19} \text{ cm}^{-2}$  and redshift  $z = 1.41$  for ISCS J1438.1+3414, we derive a gas temperature of  $3.3^{+1.9}_{-1.0} \text{ keV}$  and a Galactic absorption corrected soft (0.5 – 2 keV) X-ray flux of  $S_{0.5-2} =$

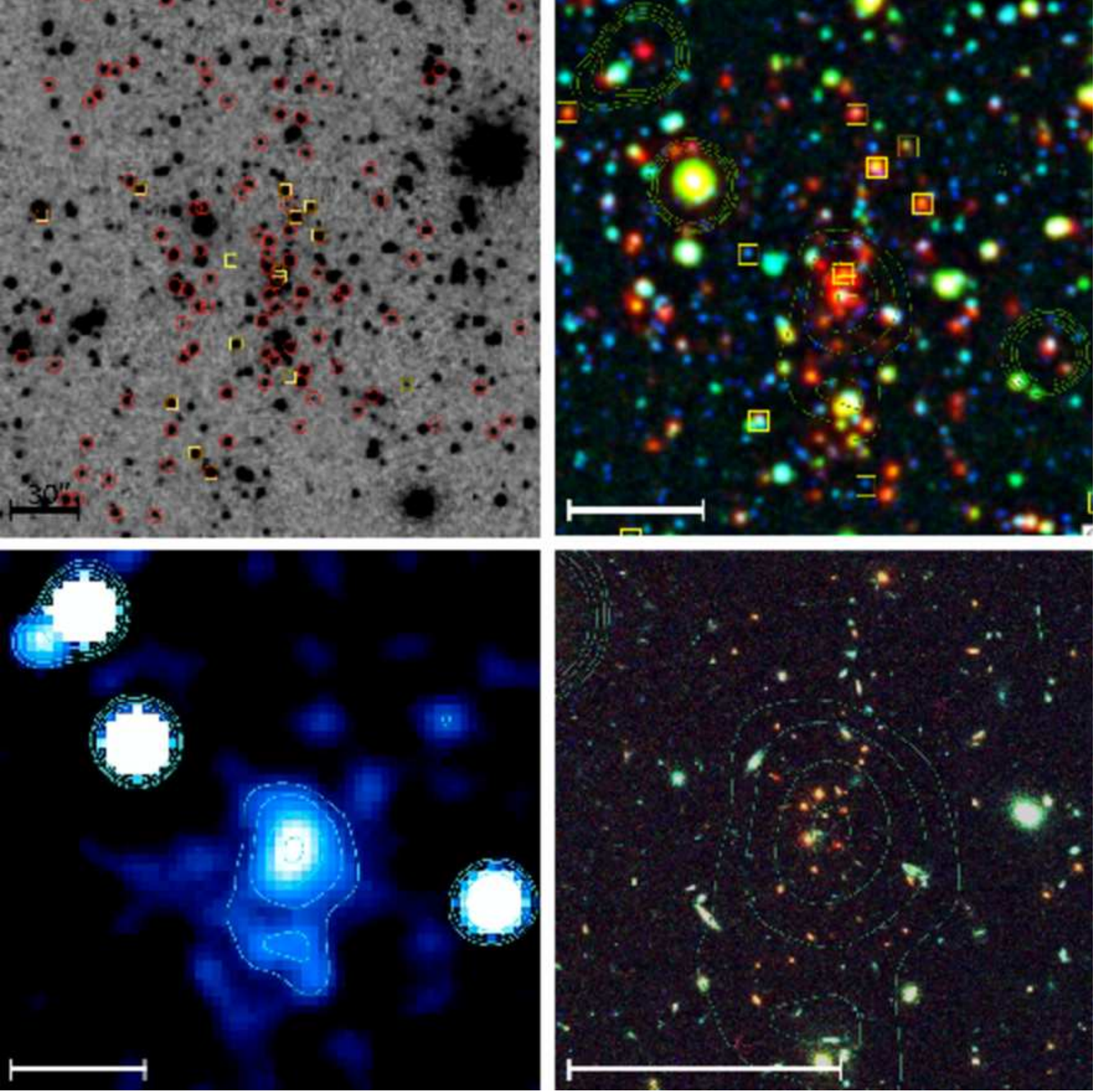


FIG. 1.— *Spitzer*, *Chandra*, and *HST* and KPNO images of ISCS J1438.1+3414 at  $z = 1.414$ . *Upper left panel*:  $4' \times 4'$  ( $\approx 2 \times 2$  Mpc) IRAC  $4.5\mu\text{m}$  image from the *Spitzer* Deep, Wide-Field Survey (SDWFS; Ashby et al. 2009), with photometric (red circles) and spectroscopic (yellow boxes) redshifts indicated. A galaxy is deemed a photometric redshift member if the integral of its redshift probability function about the cluster redshift exceeds 0.3 (see Eisenhardt et al. 2008 for details). The overdensity in stellar mass at  $z \sim 1.4$  is apparent. *Upper right panel*: Pseudo-color optical ( $B_W I$ ) + IRAC ( $4.5\mu\text{m}$ ) image of the central  $2'$  ( $\approx 1$  Mpc). The contours are from the X-ray image shown in the panel at lower left. The peak of the X-ray emission and the IRAC wavelet centroid are within  $5''$  of each other. *Lower left panel*: Binned ( $4 \times 4$ ) *Chandra* image in the 0.7–2.0 keV energy band of the central  $\approx 1$  Mpc region of ISCS J1438.1+3414. The contours correspond to 0.60, 0.75, 1.05 and 1.40 counts per  $2'' \times 2''$  pixel in this energy range in 144.2 ks. *Lower right panel*: The cluster core,  $1'$  ( $\approx 0.5$  Mpc) across centered on the X-ray centroid, shown in high resolution *HST* images (ACS/F775W, ACS/F850LP, and WFC3/F160W). The X-ray contours lie on top of the red, early type galaxies in the core of ISCS J1438.1+3414. A  $30''$  scale bar is given in each panel.

TABLE 1  
SPECTROSCOPIC CLUSTER MEMBERS

ID	R.A. (J2000)	Decl. (J2000)	z	$\Delta z$	Instrument	UT Date	Exposure Time (s)	Reference
ISCS J1438.1+3414; $\langle z \rangle = 1.414$								
J143803.7+341328	14:38:03.72	34:13:28.2	1.410	0.009	<i>HST</i> /WFC3	22 May 2010	2011	1,2
J143807.2+341446	14:38:07.26	34:14:46.3	1.410	0.009	<i>HST</i> /WFC3	22 May 2010	2011	1,2
J143807.9+341330	14:38:07.90	34:13:30.7	1.426	0.009	<i>HST</i> /WFC3	22 May 2010	2011	1,2
J143808.1+341453	14:38:08.18	34:14:53.6	1.398	0.009	<i>HST</i> /WFC3	22 May 2010	2011	1,2
J143808.3+341415	14:38:08.30	34:14:15.1	1.420	0.009	<i>HST</i> /WFC3	22 May 2010	2011	1,2
J143809.8+341345	14:38:09.83	34:13:45.0	1.423	0.009	<i>HST</i> /WFC3	22 May 2010	2011	1,2
J143810.0+341421	14:38:10.08	34:14:21.8	1.401	0.009	<i>HST</i> /WFC3	22 May 2010	2011	1,2
J143808.3+341417	14:38:08.36	34:14:17.8	1.418	0.001	Keck/DEIMOS	5 April 2007	12600	3,4,5
J143810.6+341247	14:38:10.64	34:12:47.3	1.411	0.001	Keck/DEIMOS	5 April 2007	12600	3,4,5
J143815.7+341659	14:38:15.79	34:16:59.4	1.412	0.001	Keck/DEIMOS	5 April 2007	12600	3
J143816.4+341625	14:38:16.41	34:16:25.7	1.414	0.001	Keck/DEIMOS	5 April 2007	12600	3
J143816.8+341440	14:38:16.84	34:14:40.4	1.412	0.001	Keck/DEIMOS	5 April 2007	12600	3
J143806.9+341433	14:38:06.97	34:14:33.8	1.415	0.001	Keck/LRIS	4 June 2005	12600	6
J143807.8+341441	14:38:07.80	34:14:41.6	1.417	0.001	Keck/LRIS	4 June 2005	12600	6
J143811.2+341256	14:38:11.24	34:12:56.2	1.417	0.001	Keck/LRIS	4 June 2005	12600	6
J143812.0+341318	14:38:12.09	34:13:18.2	1.415	0.001	Keck/LRIS	4 June 2005	12600	6
J143813.3+341452	14:38:13.36	34:14:52.9	1.403	0.001	Keck/LRIS	4 June 2005	12600	6
ISCS J1432.4+3250; $\langle z \rangle = 1.487$								
J143225.5+325042	14:32:25.59	32:50:42.3	1.499	0.009	<i>HST</i> /WFC3	9 Feb 2010	2011	1,2
J143221.9+324939	14:32:21.96	32:49:39.5	1.479	0.001	Keck/LRIS	11 May 2010	3600	1,7
J143232.2+324950	14:32:32.27	32:49:50.2	1.485	0.001	Keck/LRIS	11 May 2010	3600	1,7
J143222.6+325221	14:32:22.60	32:52:21.6	1.483	0.001	Keck/LRIS	11 May 2010	5400	1,7
J143223.6+325032	14:32:23.69	32:50:32.7	1.479	0.001	Keck/LRIS	11 May 2010	5400	1,7
J143224.4+324933	14:32:24.48	32:49:33.6	1.486	0.001	Keck/LRIS	11 May 2010	5400	1,7
J143225.3+325121	14:32:25.38	32:51:21.9	1.496	0.001	Keck/LRIS	11 May 2010	5400	1,7
J143225.6+325043	14:32:25.60	32:50:43.3	1.493	0.001	Keck/LRIS	11 May 2010	5400	1,7

REFERENCES. — 1 (This Work); 2 (Stanford et al. in prep); 3 (Eisenhardt et al. 2008); 4 (Dawson et al. 2009); 5 (Barbary et al. 2010); 6 (Stanford et al. 2005); 7 (Brodwin et al. in prep).



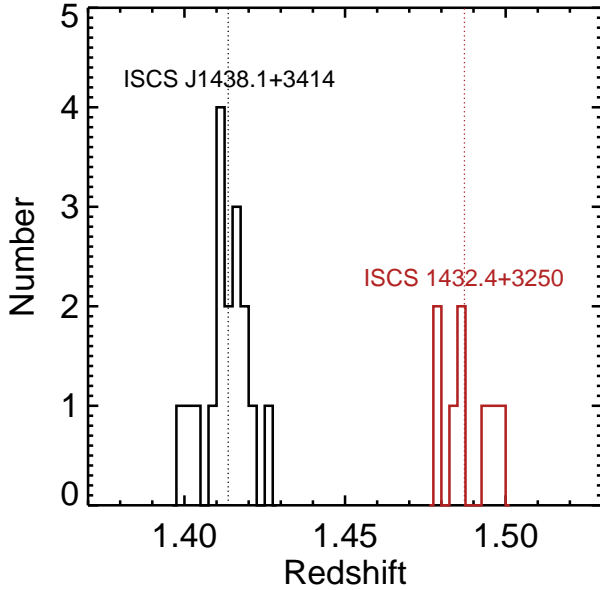


FIG. 2.— Spectroscopic redshift histogram of confirmed members in clusters ISCS J1438.1+3414 (black) and ISCS J1432.4+3250 (red). The well-sampled redshift distribution in ISCS J1438.1+3414 appears to trace a single massive halo with Gaussian-distributed velocities.

$9.0^{+2.1}_{-1.7} \times 10^{-15} \text{ erg cm}^{-2} \text{ s}^{-1}$ . These errors represent the 68% confidence interval. Markevitch (1998) report that temperature biases that arise in cool-core clusters can be minimized by excluding the central 70 kpc from the fit. We have verified that the excising the core has no significant effect on the measured temperature in ISCS J1438.1+3414. The corresponding rest-frame soft X-ray luminosity for our adopted cosmology is  $L_{0.5-2} = 1.00^{+0.24}_{-0.19} \times 10^{44} \text{ erg s}^{-1}$ .

Adopting the  $M_{500} - L_X$  relation of Vikhlinin et al. (2009), we derive a luminosity-based total mass of  $\log(M_{500,L_X}/M_\odot) = 14.17^{+0.11}_{-0.14}$ . To estimate a total virial mass, we assume an NFW density profile (Navarro et al. 1997) and the mass-concentration relation of Duffy et al. (2008), finding  $M_V \approx M_{200,L_X} = 1.54 M_{500,L_X}$ . Therefore,  $\log(M_{200,L_X}/M_\odot) = 14.35^{+0.11}_{-0.14}$ . We also infer the mass from the  $M_{500} - T_X$  relation of Vikhlinin et al. (2009), which has a lower intrinsic scatter than the luminosity-mass relation and hence provides a useful consistency check. The  $T_X$ -based mass is  $\log(M_{200,T_X}/M_\odot) = 14.2^{+0.3}_{-0.4}$ .

### 3.2. ISCS J1432.4+3250

We measure 42 background-subtracted source counts for cluster ISCS J1432.4+3250, corresponding to a detection significance of  $5.2\sigma$ . The X-ray peak is centered at  $\alpha = 14^h 32^m 24.2^s$ ,  $\delta = 32^\circ 49' 55''$  (J2000). Adopting a Galactic  $N_H = 8.71 \times 10^{19} \text{ cm}^{-2}$  and redshift  $z = 1.49$  for ISCS J1438.1+3414, we derive a poorly constrained gas temperature  $T_X \sim 2.6 \text{ keV}$  and a Galactic absorption corrected soft X-ray flux of  $S_{0.5-2} = 1.0^{+0.8}_{-0.5} \times 10^{-14} \text{ erg cm}^{-2} \text{ s}^{-1}$ . The corresponding rest-frame soft X-ray luminosity is  $L_{0.5-2} = 1.3^{+1.1}_{-0.6} \times 10^{44} \text{ erg s}^{-1}$ , from which we infer a total mass

TABLE 2  
COMPARISON OF DYNAMICAL AND X-RAY MASSES

Property	ISCS J1438.1+3414	ISCS J1432.4+3250
$z$	1.414	1.487
$\sigma \text{ (km s}^{-1}\text{)}$	$757^{+247}_{-208}$	-
$L_X \text{ (} 10^{44} \text{ erg s}^{-1}\text{)}$	$1.00^{+0.24}_{-0.19}$	$1.3^{+1.1}_{-0.6}$
$T_X \text{ (keV)}$	$3.3^{+1.9}_{-1.0}$	-
$\log(M_{200,\text{dyn}}/M_\odot)$	$14.4^{+0.3}_{-0.7}$	-
$\log(M_{200,L_X}/M_\odot)$	<b><math>14.35^{+0.11}_{-0.14}</math></b>	<b><math>14.4 \pm 0.2</math></b>
$\log(M_{200,T_X}/M_\odot)$	$14.2^{+0.3}_{-0.4}$	-

of  $\log(M_{200,L_X}/M_\odot) = 14.4 \pm 0.2$ .

## 4. DISCUSSION

### 4.1. Comparison of Mass Measures

In the preceding sections we presented dynamical and X-ray measures of the total masses of clusters ISCS J1438.1+3414 and ISCS J1432.4+3250. The large number of spectroscopic redshifts and deep X-ray imaging available for ISCS J1438.1+3414 allows a comparison of these masses, and therefore, a quantitative characterization of the ISCS cluster selection at  $z \sim 1.4$ . As the data for ISCS J1432.4+3250 are not yet of the same quality, we make a more qualitative mass comparison for this cluster.

A summary of the measured masses is presented in Table 2. The luminosity-based X-ray mass for ISCS J1438.1+3414 is in excellent agreement with both the dynamical and  $T_X$ -based masses. This suggests that the  $L_X$ -based mass,  $\log(M_{200,L_X}/M_\odot) = 14.35^{+0.11}_{-0.14}$ , is unbiased and we take it as our final mass estimate for ISCS J1438.1+3414. While the sparse redshift sampling of ISCS J1432.4+3250 precludes a direct dynamical mass measurement, the velocity distribution is similar to that of ISCS J1438.1+3414. The  $L_X$ -based mass,  $\log(M_{200,L_X}/M_\odot) = 14.4 \pm 0.2$ , is consistent with the qualitative expectation from these velocities and confirms that ISCS J1432.4+3250 is a similarly massive cluster.

### 4.2. $\sigma - T_X$ Relation

There is a well-known correlation between X-ray temperature and galaxy velocity dispersion for galaxy clusters (Lubin and Bahcall 1993; Bird et al. 1995; Girardi et al. 1996; Horner et al. 1999; Xue and Wu 2000; Ortiz-Gil et al. 2004). Although this relation was defined at low redshift, there is no expectation of, nor evidence for, evolution in this relation to  $z \sim 1$  (e.g., Wu et al. 1998; Tran et al. 1999; Brodwin et al. 2010).

Figure 4 plots ISCS J1438.1+3414 on this  $\sigma - T_X$  relation (large red circle). At  $z = 1.414$ , this is the most distant cluster for which this relation has ever been tested. A comparison sample of low redshift ( $z < 0.1$ ) clusters is plotted, along with the most massive spectroscopically confirmed cluster at  $z > 1$ , SPT-CL J0546-5345 from Brodwin et al. (2010). The dashed line is the best-fit relation Girardi et al. (1996) obtained using previous temperatures from the literature, and the solid line is our own fit using the Vikhlinin et al. (2009) temperatures for the low- $z$  clusters. ISCS J1438.1+3414 is clearly consistent with this relation. We conclude

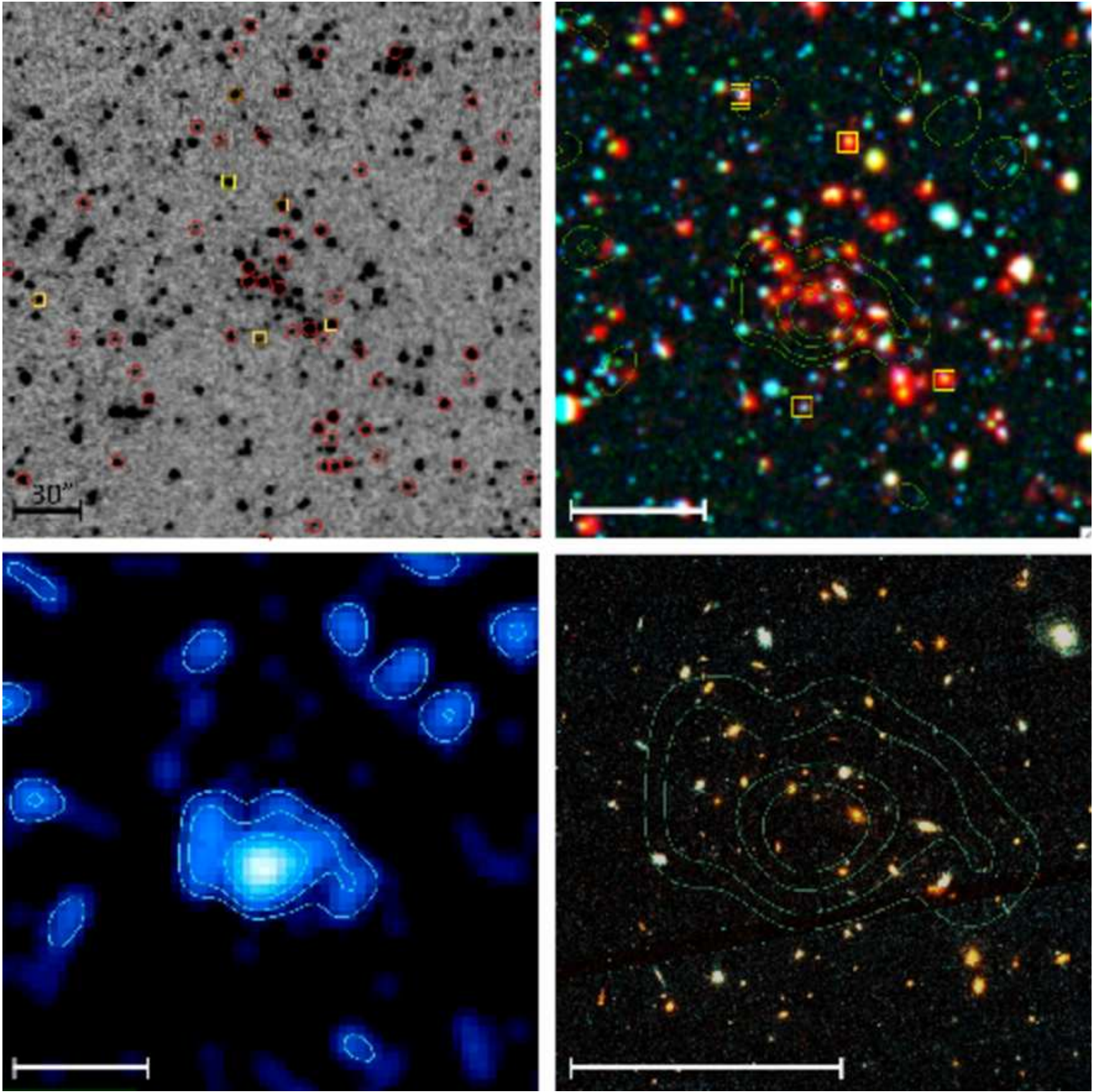


FIG. 3.— Same as for Figure 1, but for cluster ISCS J1432.4+3250 at  $z = 1.487$ . The X-ray contours correspond to 0.06, 0.09, 0.15 and 0.21 counts per  $2'' \times 2''$  pixel per 31.1 ks in the 0.7-2 keV band. The pseudo-color *HST* image in the lower right panel is composed of ACS/F814W and WFC3/F160W images.

that it is similar in nature to massive clusters selected in the X-ray or SZE. In particular, it is not underluminous in the X-ray relative to its dynamical properties, as has been suggested of some optically selected clusters at lower redshifts (Bower et al. 1994; Donahue et al. 2001; Gilbank et al. 2004; Popesso et al. 2007).

#### 4.3. Systematic Uncertainties

Total cluster masses inferred from dynamical or X-ray observables are subject to various systematic uncertainties. Here we briefly explore how these might affect our derived cluster masses.

##### 4.3.1. Dynamical Mass Systematics

**Galaxies as Tracers of the Potential** While cluster galaxies are found in simulations to be unbiased tracers of the gravitational potential (e.g., Evrard et al. 2008, and references therein), observations of low redshift clusters indicate that emission line galaxies (ELGs) may produce dispersions  $\sim 10\%$  higher than those measured from quiescent galaxies (e.g., Girardi et al. 1996; Biviano et al. 1997; de Theije and Katgert 1999; Sodre et al. 1989). This is thought to be primarily due to the influence of infalling field galaxies which have not fully virialized. Of the spectroscopic members in ISCS J1438.1+3414,

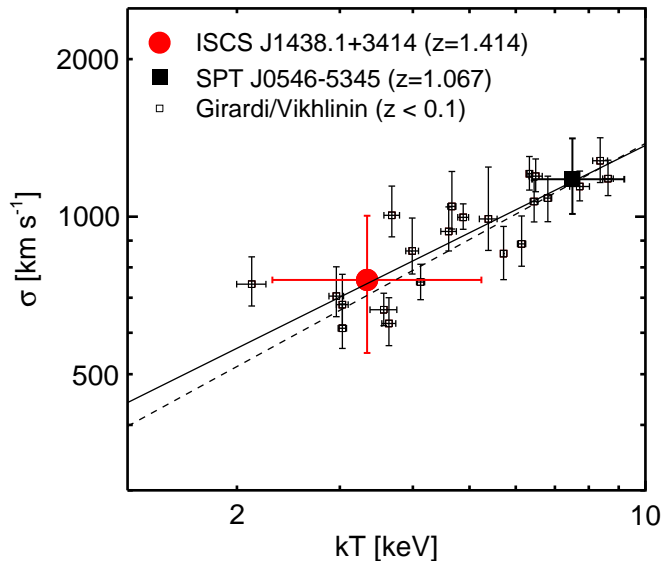


FIG. 4.— Empirical  $\sigma - T_X$  correlation for the X-ray clusters from Vikhlinin et al. (2009), with velocity dispersions taken from Girardi et al. (1996). The filled black square shows the result for SPT-CL J0546-5345, a massive SZE-selected cluster at  $z = 1.067$  (Brodwin et al. 2010). The fits, described in the text, are typical of those found by other authors (e.g., Lubin and Bahcall 1993; Horner et al. 1999). ISCS J1438.1+3414 (red circle) is clearly consistent with this relation.

11/17 were secured via emission features, so this is a possible source of systematic uncertainty. However, high star formation rates are observed in clusters at  $z \sim 1.5$  (Hilton et al. 2010; Tran et al. 2010), including amongst the central, massive members in the cluster cores. Indeed, the central galaxies in ISCS J1438.1+3414 have very high star formation rates, as inferred from *Spitzer*  $24\mu\text{m}$  observations (Brodwin et al. in prep). This suggests that the simple interpretation of ELGs as tracers of the infalling galaxy population is likely at least partially incorrect in ISCS J1438.1+3414. It is therefore not straightforward to quantify the possible bias in the dispersion due to the population mix at such high redshift, but it is likely  $< 10\%$ . This is much smaller than the statistical errors and would not affect any of the conclusions presented here.

**The Virial Approximation** Cluster mass estimates based upon velocity dispersions are predicated upon the assumption of virial equilibrium, yet for systems at high redshift and with disturbed X-ray morphologies like ISCS J1438.1+3414 it is not *a priori* obvious that this approximation is reasonable. In general, departures from virial equilibrium tend to bias mass estimates upward due to the inclusion of infalling structures with bulk motions. We cannot discount the possibility that for this system the dispersion is impacted by non-virial motion. The agreement between the dynamical, lensing, and ICM mass determinations, however, argues that the systematic bias from this effect is not large.

**Impact of Radial Sampling** The observed galaxy cluster velocity dispersion is sensitive to the radius over which it is measured since the line-of-sight dispersion decreases with radius. The radius  $r_{200}$ , where the overdensity is 200 times the critical density, is the op-

timal radius within which to measure the dispersion for determination of  $M_{200}$  (e.g., Katgert et al. 1996, 1998; Rines and Diaferio 2006; Biviano et al. 2006). In ISCS J1438.1+3414 our spectroscopy extends to  $\sim 1.5r_{200}$ , where we estimate  $r_{200} = 1.05^{+0.27}_{-0.20}$  Mpc following Carlberg et al. (1997). According to the simulations of Biviano et al. (2006), this may produce an underestimate of the dispersion by  $\sim 6\%$ . This is both small and in the opposite sense as the possible bias due to the population mix, and therefore should not materially affect our results.

#### 4.3.2. X-ray Mass Systematics

**Evolution of Scaling Relations** The primary systematic uncertainty in deriving total masses from the X-ray observables of temperature and luminosity arises from possible evolution in the temperature- and luminosity-mass scaling relations. These relations have been calibrated primarily at moderate ( $z \lesssim 0.6$ ) redshift (Maughan 2007; Vikhlinin et al. 2009; Mantz et al. 2010), and possible evolutionary effects at  $z > 1$  are untested. We therefore simply note that ISCS J1438.1+3414 and ISCS J1432.4+3250 provide valuable additions to the handful of spectroscopically confirmed  $z > 1.4$  clusters with X-ray detections (e.g., Stanford et al. 2006; Papovich et al. 2010; Tanaka et al. 2010; Gobat et al. 2010).

**Cluster Dynamical State** Another possible systematic issue arises from the dynamical state of these high redshift clusters. As Figures 1 and 3 illustrate, the X-ray morphologies of ISCS J1438.1+3414 and ISCS J1432.4+3250 are unrelaxed, showing the filamentary structure and isophotal centroid shifts (e.g., Mohr et al. 1993) typical of most high redshift clusters (Vikhlinin et al. 2009). Using high-resolution numerical simulations, Kravtsov et al. (2006) conclude that the  $M_{500} - T_X$  relation may underestimate cluster mass by  $\sim 20\%$  in such unrelaxed clusters, and therefore the temperature-based mass for ISCS J1438.1+3414 may be underestimated at this level. Given the considerable uncertainties in these scaling relations at  $z > 1$  we opt not to apply this correction, but simply note that it would bring the  $T_X$ -based mass into even closer agreement with the other mass measures.

## 5. CONCLUSIONS

We present X-ray observations of two  $z > 1.4$  spectroscopically confirmed galaxy clusters from the ISCS. ISCS J1438.1+3414, at  $z = 1.414$ , is detected in deep *Chandra* data at a significance of  $9.7\sigma$ . We measure a luminosity of  $L_{0.5-2} = 1.00^{+0.24}_{-0.19} \times 10^{44}$  erg s $^{-1}$  and a temperature of  $T_x = 3.34^{+1.90}_{-1.04}$  keV. From these we derive total  $L_X$ - and  $T_X$ -based masses of  $\log(M_{200,L_X}/M_\odot) = 14.35^{+0.11}_{-0.14}$  and  $\log(M_{200,T_X}/M_\odot) = 14.2^{+0.3}_{-0.4}$ . These agree with the dynamical mass, inferred from 17 spectroscopically confirmed members, of  $\log(M_{200,\text{dyn}}/M_\odot) = 14.4^{+0.3}_{-0.7}$ . The X-ray and dynamical properties of ISCS J1438.1+3414 are fully consistent with the  $\sigma - T_X$  relation. This is the most distant cluster for which this relation has been tested.

We also present spectroscopic confirmation for ISCS J1432.4+3250 at  $z = 1.487$ , the most distant



of 18  $z > 1$  clusters confirmed in the ISCS to date. ISCS J1432.4+3250 is detected at a  $5.2\sigma$  significance in a shallow *Chandra* exposure. We measure an X-ray luminosity of  $L_{0.5-2} = 1.3_{-0.6}^{+1.1} \times 10^{44}$  erg s $^{-1}$ , from which we infer a total mass of  $\log(M_{200,LX}/M_{\odot}) = 14.4 \pm 0.2$ . The sparse dynamical data are consistent with this X-ray mass, confirming that ISCS J1432.4+3250 is also a massive high redshift cluster.

Our primary conclusion is that the  $z \gtrsim 1.4$  clusters studied in this work, identified by the stellar-mass selection of the ISCS, are massive and have dynamical and ICM properties typical of clusters selected by the X-ray or SZE. This further confirms that stellar-mass cluster selection provides a powerful and sensitive method for studying cluster evolution to the highest redshifts. The two clusters presented in this work, with total masses of  $\log(M_{200}/M_{\odot}) \approx 14.4$  or  $\approx 2 - 3 \times 10^{14} M_{\odot}$ , are nearly Coma-mass progenitors. The ISCS is therefore identifying the precursor population of present-day massive clusters.

This work is based in part on observations obtained with the *Chandra X-ray Observatory* (CXO), under contract SV4-74018, A31 with the Smithsonian Astrophysical Observatory which operates the CXO for NASA. Support for this research was provided by NASA grant G09-0150A. This work is based in part on observations made with the *Spitzer Space Telescope*, which is operated by the Jet Propulsion Laboratory, California Institute of Technology under a contract with NASA. Support for this work was provided by NASA through an award is-

sued by JPL/Caltech. This work is based, in part, on observations made with the NASA/ESA *Hubble Space Telescope*, obtained at the Space Telescope Science Institute, which is operated by the Association of Universities for Research in Astronomy, Inc., under NASA contract NAS 5-26555. These observations are associated with programs 11597 and 11663. Support for programs 11597 and 11663 were provided by NASA through a grant from the Space Telescope Science Institute, which is operated by the Association of Universities for Research in Astronomy, Inc., under NASA contract NAS 5-26555. Some of the data presented herein were obtained at the W. M. Keck Observatory, which is operated as a scientific partnership among the California Institute of Technology, the University of California and the National Aeronautics and Space Administration. The Observatory was made possible by the generous financial support of the W. M. Keck Foundation. This work makes use of image data from the NOAO Deep Wide-Field Survey (NDWFS) and the Deep Lens Survey (DLS) as distributed by the NOAO Science Archive. NOAO is operated by the Association of Universities for Research in Astronomy (AURA), Inc., under a cooperative agreement with the National Science Foundation.

This paper would not have been possible without the efforts of the *Spitzer*, *Chandra*, *HST* and Keck support staff. Support for MB was provided by the W. M. Keck Foundation. The work by SAS at LLNL was performed under the auspices of the U. S. Department of Energy under Contract No. W-7405-ENG-48.

## REFERENCES

- Andreon, S. 2008, in *Chandra Proposal 2662*
- Ashby, M. L. N., et al. 2009, *ApJ*, **701**, 428
- Barbary, K., et al. 2010, *ApJ*, submitted (arXiv:1010.5786)
- Beers, T. C., Flynn, K., and Gebhardt, K. 1990, *AJ*, **100**, 32
- Bird, C. M., Mushotzky, R. F., and Metzler, C. A. 1995, *ApJ*, **453**, 40
- Biviano, A., Katgert, P., Mazure, A., Moles, M., den Hartog, R., Perea, J., and Focardi, P. 1997, *A&A*, **321**, 84
- Biviano, A., Murante, G., Borgani, S., Diaferio, A., Dolag, K., and Girardi, M. 2006, *A&A*, **456**, 23
- Bower, R. G., Bohringer, H., Briel, U. G., Ellis, R. S., Castander, F. J., and Couch, W. J. 1994, *MNRAS*, **268**, 345
- Brodwin, M., et al. 2006, *ApJ*, **651**, 791
- Brodwin, M., Gonzalez, A. H., Moustakas, L. A., Eisenhardt, P. R., Stanford, S. A., Stern, D., and Brown, M. J. I. 2007, *ApJ*, **671**, L93
- Brodwin, M., et al. 2010, *ApJ*, **721**, 90
- Carlberg, R. G., Yee, H. K. C., and Ellingson, E. 1997, *ApJ*, **473**, 462
- Danese, L., de Zotti, G., and di Tullio, G. 1980, *A&A*, **82**, 322
- Dawson, K. S., et al. 2009, *AJ*, **138**, 1271
- de Heije, P. A. M. and Katgert, P. 1999, *A&A*, **341**, 371
- Donahue, M., et al. 2001, *ApJ*, **552**, L93
- Duffy, A. R., Schaye, J., Kay, S. T., and Dalla Vecchia, C. 2008, *MNRAS*, **390**, L64
- Eisenhardt, P. R. M., et al. 2008, *ApJ*, **684**, 905
- Elston, R. J., et al. 2006, *ApJ*, **639**, 816
- Evvard, A. E., et al. 2008, *ApJ*, **672**, 122
- Faber, S. M., et al. 2003, in *Instrument Design and Performance for Optical/Infrared Ground-based Telescopes. Edited by Iye, Masanori; Moorwood, Alan F. M. Proceedings of the SPIE, Volume 4841, pp. 1657-1669 (2003).*, pp 1657-1669
- Gilbank, D. G., Bower, R. G., Castander, F. J., and Ziegler, B. L. 2004, *MNRAS*, **348**, 551
- Girardi, M., Fadda, D., Giuricin, G., Mardirossian, F., Mezzetti, M., and Biviano, A. 1996, *ApJ*, **457**, 61
- Gobat, R., et al. 2010, *A&A* submitted (arXiv:1011.1837)
- Hilton, M., et al. 2010, *ApJ*, **718**, 133
- Horner, D. J., Mushotzky, R. F., and Scharf, C. A. 1999, *ApJ*, **520**, 78
- Jannuzi, B. T. and Dey, A. 1999, in *ASP Conf. Ser. 191 — Photometric Redshifts and the Detection of High Redshift Galaxies*, p. 111
- Katgert, P., Mazure, A., den Hartog, R., Adami, C., Biviano, A., and Perea, J. 1998, *A&AS*, **129**, 399
- Katgert, P., et al. 1996, *A&A*, **310**, 8
- Komatsu, E., et al. 2010, *ApJS*, submitted (arXiv:1001.4538)
- Kravtsov, A. V., Vikhlinin, A., and Nagai, D. 2006, *ApJ*, **650**, 128
- Kubo, J. M., Stebbins, A., Annis, J., Dell'Antonio, I. P., Lin, H., Khiabani, H., and Frieman, J. A. 2007, *ApJ*, **671**, 1466
- Kümmel, M., Walsh, J. R., Pirzkal, N., Kuntschner, H., and Pasquali, A. 2009, *PASP*, **121**, 59
- Lubin, L. M. and Bahcall, N. A. 1993, *ApJ*, **415**, L17
- Mantz, A., Allen, S. W., Ebeling, H., Rapetti, D., and Drlica-Wagner, A. 2010, *MNRAS*, **406**, 1773
- Markevitch, M. 1998, *ApJ*, **504**, 27
- Maughan, B. J. 2007, *ApJ*, **668**, 772
- Mewe, R., Gronenschild, E. H. B. M., and van den Oord, G. H. J. 1985, *A&AS*, **62**, 197
- Mohr, J. J., Fabricant, D. G., and Geller, M. J. 1993, *ApJ*, **413**, 492
- Morrison, R. and McCammon, D. 1983, *ApJ*, **270**, 119
- Murray, S. S., et al. 2005, *ApJS*, **161**, 1
- Navarro, J. F., Frenk, C. S., and White, S. D. M. 1997, *ApJ*, **490**, 493
- Oke, J. B., et al. 1995, *PASP*, **107**, 375
- Ortiz-Gil, A., Guzzo, L., Schuecker, P., Böhringer, H., and Collins, C. A. 2004, *MNRAS*, **348**, 325



- Papovich, C., et al. 2010, *ApJ*, **716**, 1503
- Popesso, P., Biviano, A., Böhringer, H., and Romaniello, M. 2007, *A&A*, **461**, 397
- Rines, K. and Diaferio, A. 2006, *AJ*, **132**, 1275
- Sodre, Jr., L., Capelato, H. V., Steiner, J. E., and Mazure, A. 1989, *AJ*, **97**, 1279
- Stanford, S. A., et al. 2005, *ApJ*, **634**, L129
- Stanford, S. A., et al. 2006, *ApJ*, **646**, L13
- Tanaka, M., Finoguenov, A., and Ueda, Y. 2010, *ApJ*, **716**, L152
- Tran, K., Kelson, D. D., van Dokkum, P., Franx, M., Illingworth, G. D., and Magee, D. 1999, *ApJ*, **522**, 39
- Tran, K., et al. 2010, *ApJ*, **719**, L126
- Vikhlinin, A., et al. 2009, *ApJ*, **692**, 1033
- Wu, X., Chiueh, T., Fang, L., and Xue, Y. 1998, *MNRAS*, **301**, 861
- Xue, Y. and Wu, X. 2000, *ApJ*, **538**, 65